Generalized Dispersion Analysis and Spurious Modes of 2-D and 3-D TLM Formulations

John S. Nielsen, *Member, IEEE,* and Wolfgang J. R. Hoefer, *Fellow, IEEE*

***Abstract*—The general dispersion relations are derived for the 2-D TLM shunt and series meshes and the 3-D TLM expanded and condensed node meshes. Implicit in the resulting dispersion relations are both their physical and spurious modal solutions. It is demonstrated that of the four schemes, only the 3-D expanded node mesh is free of detrimental spurious solutions.**

I. Introduction

In terms of numerical dispersion effects, the Transmission Line Matrix (TLM) method is similar to Finite Difference Time Domain (FD-TD) and Finite Element (FE) methods based on approximations of the single curl Maxwell equations. A review of the numerical dispersion and spurious modes supported by the FD-TD and FE methods is given by [1] and [2]. Significant effort has been expended on the development of spurious free FE algorithms. A recently proposed method was given by Boyse *et al.* [3].

The Transmission Line Matrix (TLM) method, originally developed by Johns [4], is a means of simulating the time domain solution of electromagnetic fields by a procedure of recursive calculations that are updated at regular time intervals. It can be demonstrated that these recursive relations are equivalent to a finite difference approximation of Maxwell's equations [5]–[7].

The work of Brewitt–Taylor and Johns [8] was brought to our attention by the reviewer, as the original analysis of the dispersion characteristics of the TLM mesh. A limitation of this analysis procedure is that an equivalent circuit model of the TLM node is required. As a practical equivalent circuit model for the 3-D symmetrical condensed node has not been developed, the general dispersion relation was not derived except for special cases such as propagation along the axis or diagonal [9]. The general dispersion relation was later derived by Nielsen and Hoefer [10], which further led to the characterization of spurious modes of the condensed node [11].

In this paper, a method is described which enables the dispersion relation of an arbitrary TLM node to be derived based on the scattering matrix of the node without the requirement of an equivalent circuit. This method has been used to evaluate the dispersion and spurious solutions of commonly used TLM meshes. In the following sections, the dispersion relation and spurious modes will be evaluated for the 2-D shunt node, 2-D series node, 3-D expanded node, and 3-D symmetrical condensed node.

Manuscript received October 29, 1992; revised January 12, 1993.

J. S. Nielsen is with the Lockheed Canada Inc., 1 Iber Rd. Stittsville, Ont., Canada K2S-1E6.

W. J. R. Hoefer is with the Department of Electrical Engineering, University of Victoria, Victoria, B.C., Canada V8W-3P6.

IEEE Log Number 9210226.

II. Types of Spurious Modes

The TLM mesh consists of an array of scattering nodes that are interconnected by transmission line links. Throughout this paper, the node spacing in all directions is assumed to be constant and equal to d. The propagation constant along the transmission lines is k_o, which is given by

$$k_o = \frac{2\pi f_o}{v_{\text{link}}} \tag{1}$$

where f_o is the excitation frequency and v_{link} is the velocity along the transmission link lines. The numerical dispersion of the mesh, at a given excitation frequency, is reduced by decreasing $k_o d$ through mesh refinement [9]. As the numerical dispersion is decreased, the overall field solution will typically converge to the physical solution. However, due to the spatial and temporal sampling process, propagating spurious modes may be supported. These spurious modes will, to some extent, corrupt the simulated field solution. Various types of spurious modes can be identified. These have been arbitrarily classified under four types for convenience as follows:

Type	Temporal Frequency	Spatial Frequency	TLM Mesh Supporting Spurious Mode Type
1	0 high	all	2-D series and shunt 3-D condensed
2	$k_o d = \pi$ low	all	2-D series and shunt 3-D condensed
3	$k_o d < \pi/2$ high	high	3-D condensed
4	$k_o d >= \pi/2$	0	3-D expanded

The nature of these spurious solutions will become evident as examples are given.

Since the TLM method is only accurate for low values of $k_o d$, it is generally not applied to problems where $k_o d$ exceeds about 0.25. Hence, low-pass temporal filtering of embedded sources can be used to suppress the spurious solutions of types 2 and 4. Spurious solutions of type 1 can be controlled by careful attention to initial conditions and placement of sources and lumped devices within the mesh as will be discussed further. Type 3 is particularly troublesome and is unfortunately supported by the 3-D condensed node mesh.

Types 1 and 3 will be referred to in this paper as "low-frequency spurious modes."

III. 2-D TLM Shunt Node

The 2-D shunt node sketched in Fig. 1(a) can represent three field components, for example, E_y, H_x, and H_z. The shunt node is formed by the intersection of two transmission lines of characteristic admittance Y_o. V_p^i and V_p^r are defined as the incident and reflected voltages at the node, where p denotes the transmission line number as indicated in Fig. 1. $\boldsymbol{V}^i$ and $\boldsymbol{V}^r$ are defined as the vectors of V_p^i and V_p^r, respectively, as

$$\boldsymbol{V}^i = \begin{pmatrix} V_1^i \\ V_2^i \\ V_3^i \\ V_4^i \end{pmatrix} \qquad \boldsymbol{V}^r = \begin{pmatrix} V_1^r \\ V_2^r \\ V_3^r \\ V_4^r \end{pmatrix}. \tag{2}$$

$\boldsymbol{V}^i$ and $\boldsymbol{V}^r$ are related through a scattering matrix $\boldsymbol{S}$ as

$$\boldsymbol{V}^r = \boldsymbol{S}\boldsymbol{V}^i. \tag{3}$$

$\boldsymbol{S}$ is derived directly from the transmission line equivalent in Fig. 1(a) as

$$\boldsymbol{S} = \frac{1}{2}\begin{pmatrix} -1 & 1 & 1 & 1 \\ 1 & -1 & 1 & 1 \\ 1 & 1 & -1 & 1 \\ 1 & 1 & 1 & -1 \end{pmatrix}. \tag{4}$$

The node scattering matrices for the TLM nodes are frequency independent and therefore applicable to continuous harmonic signals as discussed in [12]. If the transmission lines are approximated by lumped inductors and capacitors, as illustrated in Fig. 1(b), then a set of coupled differential equations results

$$\frac{\partial V_y}{\partial x} = -L_{\text{link}} \frac{\partial I_x}{\partial t} \tag{5a}$$

$$\frac{\partial V_y}{\partial z} = -L_{\text{link}} \frac{\partial I_z}{\partial t} \tag{5b}$$

$$\frac{\partial I_z}{\partial z} + \frac{\partial I_x}{\partial x} = -2C_{\text{link}} \frac{\partial V_y}{\partial t} \tag{5c}$$

where V_y, I_x, and I_z are indicated in Fig. 1(b). L_{link} and C_{link} are defined as the inductance and capacitance of the link line per unit length, respectively. It is readily observed that if the following equivalences are made:

$$E_y = -\frac{V_y}{d}, \qquad H_z = -\frac{I_x}{d}, \qquad H_x = \frac{I_z}{d},$$
$$\mu = L_{\text{link}}, \qquad \varepsilon = 2C_{\text{link}} \tag{6}$$

then (4) reduces to Maxwell's equations for the TE case where

$$E_x = E_z = H_y = 0, \qquad \frac{\partial}{\partial y} = 0.$$

The dispersion relation is based on evaluating the voltage at a particular node, denoted as node c, in relation to the voltages of the four adjacent nodes which are at a distance d from node c. Let V_c denote the total voltage amplitude at node c, and let V_p' denote the voltage at the adjacent node attacked to node c through the transmission line p as shown in Fig. 1(a). The dispersion relation is based on determining the interdependence between node voltages V_c and V_p'.

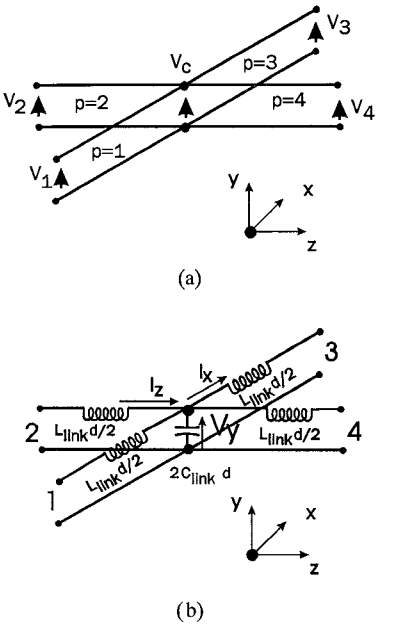

Fig. 1. 2-D TLM shunt node. (a) Node structure. (b) Equivalent LC network.

V_p' is composed of incident and reflected voltages such that

$$V_p' = V_p^{i\prime} + V_p^{r\prime} \tag{7}$$

where $V_p^{i\prime}$ is the incident voltage flowing from the adjacent node, and $V_p^{r\prime}$ is the reflected voltage flowing toward the adjacent node on the pth link line.

The dispersion relation is developed at a single excitation frequency such that

$$V_p^i = T_o V_p^{i\prime} \tag{8a}$$

$$V_p^{r\prime} = T_o V_p^r \tag{8b}$$

where T_o is given as

$$T_o = e^{-jk_o d} \tag{9}$$

where k_o is the propagation constant along the link lines defined in (1). Furthermore $\boldsymbol{V}'$, $\boldsymbol{V}^{i\prime}$, and $\boldsymbol{V}^{r\prime}$ are defined as vector forms of V_p', $V_p^{i\prime}$, and $V_p^{r\prime}$, respectively.

Defining $\boldsymbol{T}$ as

$$\boldsymbol{T} = T_o \boldsymbol{I} \tag{10}$$

where $\boldsymbol{I}$ is an identity matrix, we can write

$$\boldsymbol{V}^* = \boldsymbol{V}^{*i} + \boldsymbol{V}^{*r} = \boldsymbol{T}^{-1}\boldsymbol{V}^i + \boldsymbol{T}\boldsymbol{V}^r = \left(\boldsymbol{T}^{-1} + \boldsymbol{T}\boldsymbol{S}\right)\boldsymbol{V}^i. \tag{11}$$

Using (3), V_c can be expressed as

$$V_c = V_1^i + V_1^r = \frac{1}{2}\sum_{p=1}^{4} V_p^i. \tag{12}$$

Finally, substituting (11) into (12), we obtain an equation relating V_c to V_p' as

$$4V_c \cos(k_o d) = V_1' + V_2' + V_3' + V_4'. \tag{13}$$

Useful solutions to (13) are obtained by assuming an infinite 2-D mesh where the voltage across the node located at $x = id$ and $z = kd$ has an amplitude of

$$V_{i,k} = A_o e^{-jk_x di} e^{-jk_z dk} \tag{14}$$

where k_x and k_z are the unknown components of the mesh propagation vector, and A_o is an arbitrary constant. By substituting this solution into (13), the desired dispersion relation is obtained as

$$2\cos(k_o d) = \cos(k_x d) + \cos(k_z d)\,. \tag{15}$$

In assuming the solution of the form in (14), monochromatic excitation of the mesh is implied. The resulting dispersion relation is thus valid for monochromatic fields but not necessarily for time sampled fields composed of propagating impulse functions as is encountered in TLM. However, it can be shown that if $k_o d < \pi$, then the dispersion relation is the same for a monochromatic signal as for a time sampled version of the monochromatic signal [12].

Equation (15) can be compared to the two known dispersion relations of the shunt TLM mesh in the direction along the x- or z-axis and along the diagonal $x = z$. Consider first the case where $k_x d = 0$ which represents propagation along the z-axis. Equation (15) becomes

$$2\cos(k_o d) - 1 = \cos(k_z d) \tag{16}$$

which can be manipulated into a different form

$$\cos(k_z d) = \cos(k_o d) - \tan(k_o d/2)\sin(k_o d) \tag{17}$$

which appears in [9].

Consider next the case when the propagation is along the diagonal line $x = z$ by setting $k_x d = k_z d$. Using (15),

$$\cos(k_o d) = \cos(k_x d) = \cos(k_z d)$$

or $k_x d = K_z d = k_o d$. Consequently, the effective propagation constant along $x = z$ is nondispersive and is given by $\sqrt{2k_o}$ which is in agreement with [9].

A final observation is that (15) can also be written in the form

$$\sin^2\left(\frac{k_o d}{2}\right) = \frac{1}{2}\left(\sin^2\left(\frac{k_x d}{2}\right) + \sin^2\left(\frac{k_z d}{2}\right)\right) \tag{18}$$

which is exactly the same as the dispersion relation of the 2-D FD-TD method with a stability factor of $1/\sqrt{2}$ [2]. This equivalence between the 2-D FD-TD and 2-D TLM method has also been pointed out by Simons and Bridges [13].

Fig. 2 shows a plot of the dispersion relation (15) for various values of $k_o d$. Note that the curves are approximately circular for low values of $k_o d$, indicating negligible numerical dispersion. As $k_o d$ increases, the circles become distorted. When $k_o d$ reaches $(1/2)\pi$, the dispersion curve becomes a line given by $k_x d + k_z d = \pi$. To avoid errors due to numerical distortion, $k_o d$ is typically limited to less than 0.25.

Although spurious solutions in (15) are not evident, they do exist. Consider a shunt node surrounded by four conducting walls. Assume an incident voltage at the node given by $\boldsymbol{V}^i = [1, -1, 1, -1]^T$. From (3) and (4), $\boldsymbol{V}^r = -\boldsymbol{V}^i$. As

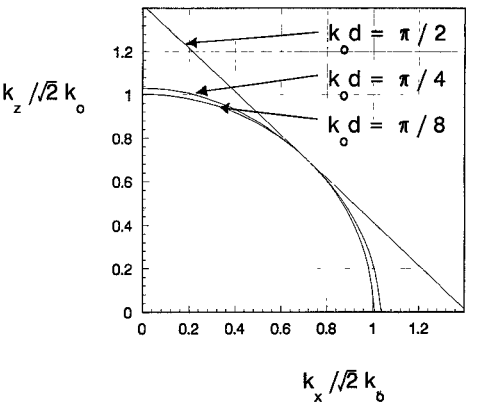

Fig. 2. Plot of the numerical dispersion of the shunt node for various values of $k_o d$.

the reflection coefficient of the conducting boundary is -1, $\boldsymbol{V}^i$ does not change in the next time interval. Hence, this case corresponds to the eigensolution of $k_x d = k_z d = \pi$ and $k_o d = 0$, which is a type 1 spurious mode. This solution was not predicted by (15) since $V_c = 0$, which can be seen by considering (12).

To obtain the complete dispersion relation, the eigenmatrix equation for $\boldsymbol{V}^i$ is derived. Assuming a solution in the form of (14) and using the port designations in Fig. 1(a), $\boldsymbol{V}^{r\prime}$ can be related to $\boldsymbol{V}^i$ through a transformation matrix $\boldsymbol{P}$ as follows:

$$\boldsymbol{V}^{r\prime} = \boldsymbol{P}\boldsymbol{V}^i \tag{19}$$

with

$$\boldsymbol{P} = \begin{pmatrix} 0 & 0 & T_x^{-1} & 0 \\ 0 & 0 & 0 & T_z^{-1} \\ T_x & 0 & 0 & 0 \\ 0 & T_z & 0 & 0 \end{pmatrix}$$

where $T_x = \exp(-jk_x d)$ and $T_z = \exp(-jk_z d)$. Also,

$$\boldsymbol{V}^{r*} = \boldsymbol{T}\boldsymbol{V}^r = \boldsymbol{T}\boldsymbol{S}\boldsymbol{V}^i\,. \tag{20}$$

By combining (19) and (20), an eigenmatrix relation is obtained as

$$(\boldsymbol{P} - \boldsymbol{T}\boldsymbol{S})\boldsymbol{V}^i = 0 \tag{21}$$

with the corresponding dispersion relation given as $\det[\boldsymbol{P}\boldsymbol{S} - \boldsymbol{t}] = 0$, as $\boldsymbol{S} = \boldsymbol{S}^{-1}$. Equation (21) can be written to highlight the eigenvalue T_o as

$$\boldsymbol{P}\boldsymbol{S}\boldsymbol{V}^i = T_o \boldsymbol{V}^i\,.$$

Hence, the solutions of $k_o d$ are related directly to the eigenvalues of the matrix $\boldsymbol{P}\boldsymbol{S}$. A plot of the eigenvalues of $\boldsymbol{P}\boldsymbol{S}$ is shown in Fig. 3 for all real values of $k_x d$ and $k_z d$. There are generally four unique eigenvalues. There is always an eigenvalue at $T_o = 1$ and $T_o = -1$ corresponding to $k_o d = 0$ and $k_o d = \pi$, respectively. These solutions correspond to spurious mode types 1 and 2, respectively. In addition, there are solutions of the form $T_o = \exp(-j\theta)$ and $T_o = \exp(j\theta)$, with θ being real which correspond to the solutions of $k_o d$ given by (15). These are called the "physical solutions" in Fig. 3. The eigenvectors of $\boldsymbol{V}^i$ corresponding to

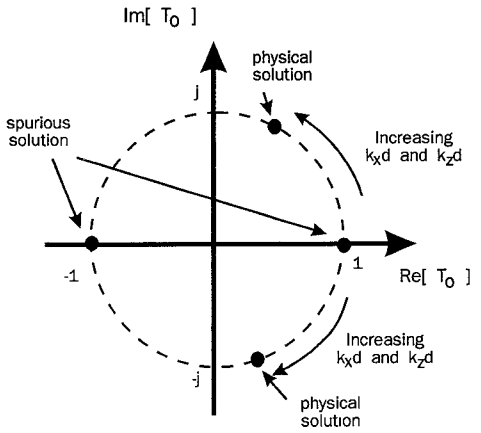

Fig. 3. Physical and spurious eigen-solutions of the shunt node in the T_o plane.

the eigenvalues $T_o = \pm 1$ depend on $k_x d$ and $k_z d$ such that $V_1^i + V_2^i + V_3^i + V_4^i = 0$ and, hence, $V_c = 0$. $\boldsymbol{V}^i = [1, -1, 1, -1]$ given above is an example of the eigen vector for $T_o = 1$. There are no spurious modes of types 3 and 4.

Since the TLM network is linear, only sources that excite frequency components corresponding to $k_o d = 0$ or $k_o d = \pi$ can couple into the spurious modes supported by the shunt node. As high-frequency excitation is avoided by bandlimiting sources, only dc sources can pose a problem. Sources that shunt the node will not couple to the dc spurious mode due to symmetry arguments. However, sources placed in the series into the link lines can potentially couple to the type 1 spurious mode.

IV. 2-D TLM Series Node

The 2-D series node is sketched in Fig. 4(a) and can represent three field components of TM modes, namely, E_x, E_z, and H_y [9]. The series node is formed by a series connection of two intersecting transmission lines of admittance Y_o resulting in a node scattering matrix of

$$\boldsymbol{S} = \frac{1}{2}\begin{pmatrix} 1 & 1 & 1 & -1 \\ 1 & 1 & -1 & 1 \\ 1 & -1 & 1 & 1 \\ -1 & 1 & 1 & 1 \end{pmatrix}. \tag{22}$$

If the transmission lines are approximated by lumped inductors and capacitors as illustrated in Fig. 4(b), then a pair of coupled differential equations emerges as

$$\frac{\partial I_y}{\partial x} = -C_{\text{link}} \frac{\partial V_z}{\partial t} \tag{23a}$$

$$\frac{\partial I_y}{\partial z} = -C_{\text{link}} \frac{\partial V_x}{\partial t} \tag{23b}$$

$$\frac{\partial V_x}{\partial z} + \frac{\partial V_z}{\partial x} = -2L_{\text{link}} \frac{\partial I_y}{\partial x} \tag{23c}$$

where I_y, V_x, and V_z are indicated in Fig. 4(b). If the following equivalences are made:

$$H_y = \frac{I_y}{d}, \qquad E_x = -\frac{V_x}{d}, \qquad E_z = \frac{V_z}{d},$$
$$\mu = 2L_{\text{link}}, \quad \varepsilon_{x,z} = C_{\text{link}}, \tag{24}$$

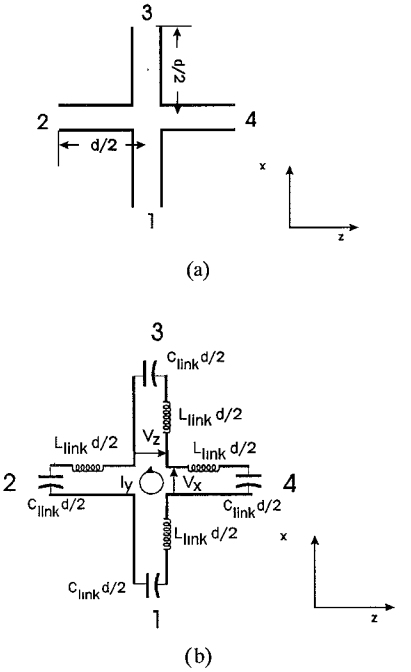

Fig. 4. 2-D TLM series node. (a) Node structure. (b) Equivalent circuit.

then (23) reduces to Maxwell's equations for the TM case with

$$H_x = H_z = E_y = 0; \qquad \frac{\partial}{\partial y} = 0.$$

The derivation of the dispersion relation for the series node is similar to the derivation followed for the shunt node. The current at the center of a series node c is related to the currents at the center of the four adjacent nodes as illustrated in Fig. 5. At the center of the adjacent nodes, the currents are denoted as J'_p where again p denotes the link line number. I_c is the value of the current flowing around the center series node in the direction indicated in Fig. 5. $\boldsymbol{J'}$, defined as the vector of J'_p, can be written as

$$\boldsymbol{J'} = Y_o\left(\boldsymbol{V}^{i\prime} - \boldsymbol{V}^{r\prime}\right). \tag{25}$$

Hence,

$$\boldsymbol{J'} = Y_o\left(\boldsymbol{T}^{-1} - \boldsymbol{TS}\right)\boldsymbol{V}^i. \tag{26}$$

The current I_c can be written in terms of V_1^i and V_2^r as

$$I = Y_o\left(V_1^i - V_1^r\right) = \frac{Y_o}{2}\left(v_1^i - v_2^i - v_3^i + v_4^i\right). \tag{27}$$

Introducing (26) in (27) yields

$$4I_c \cos\left(k_o d\right) = \left(J'_1 - J'_2 - J'_3 + J'_4\right). \tag{28}$$

As for the shunt node, the desired dispersion relation is obtained by assuming a solution of the form

$$I_{i,k} = A_o e^{-jk_x di} e^{-jk_z dk}. \tag{29}$$

Substituting this solution into (27) results in the dispersion relation

$$2\cos(k_o d) = \cos(k_x d) + \cos(k_z d) \tag{30}$$

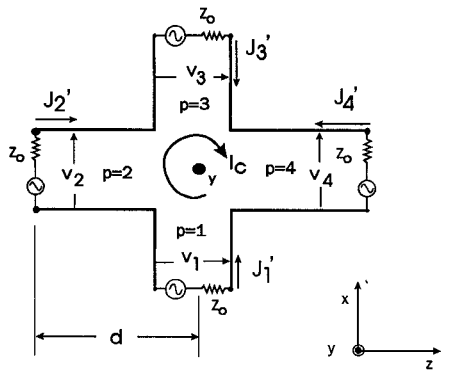

Fig. 5. Variables used in the derivation of the dispersion relation of the 2-D series node.

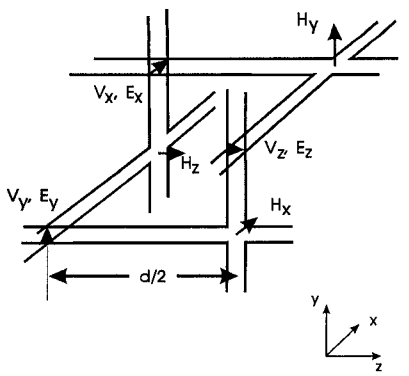

Fig. 6. 3-D TLM expanded node indicating location of sampled field quantities.

which is identical to the dispersion relation of the shunt node in (15).

As for the shunt node, there are additional spurious modes that are not visible by the dispersion relation. For example, consider the case with a series node surrounded by magnetic walls and an incident voltage vector of $\boldsymbol{V}^i = [1,1,1,1]$. As observed, this results in a self-consistent solution yielding $I_c = 0$. This solution is predicted from the eigenvalues and eigenvectors of $\boldsymbol{PS}$ as in the shunt node case resulting in the same set of four eigenvalues at ± 1, $\exp(j\theta)$ and $\exp(-j\theta)$, where θ corresponds to the values of $k_o d$ obtained from the dispersion relation (30).

V. Expanded 3-D TLM Node

Akhtarzad and Johns [14] arranged the TLM series and shunt nodes in an interlaced arrangement resulting in the 3-D expanded node as illustrated in Fig. 6. The term "expanded" is used since the evaluated field components are not collocated. Each cell of the expanded node consists of three shunt nodes representing the E_x, E_y, and E_z fields and three series nodes representing the H_x, H_y, and H_z fields. The spacing between the series and shunt nodes is $d/2$, and the overall cell size is d. The incident voltages converging on the shunt nodes are scattered at interval time steps, and the incident voltages converging on the series nodes are scattered half a time step later. Hence, the E and H fields are not updated at the same time but at half-time step intervals as in Yee's FD-TD scheme [15]. It was demonstrated by Johns [5] and by Voelker and Lomax [6] that the expanded TLM node is analogous to Yee's FD-TD node, except that the expanded node has twelve independent variables associated with each node, whereas Yee's scheme has six.

As discussed by Paulsen [1], Yee's 3-D FD-TD scheme [15] is free of spurious solutions. This is a somewhat surprising property, which is attributed to the staggered mesh configuration. The additional variables associated with the expanded TLM node result in supported spurious modes as will be demonstrated. However, these spurious modes are of type 4 which can be easily suppressed by temporal filtering. The expanded node does not support low-frequency spurious modes of types 1 or 3. This is an important advantage of the expanded node over the condensed node which does support the propagation of low-frequency spurious modes.

Two derivations of the dispersion relation were performed—one based on the voltages at the shunt nodes and the other on the currents at the series nodes. As these derivations are similar, details will only be given for the voltage based dispersion relation. Both approaches result in the same overall dispersion relation. By considering both derivations, it will be shown that there are no low-frequency spurious modes.

The voltages of the expanded node, V_x, V_y, and V_z, are represented at the three shunt nodes of the unit cell, as shown in Fig. 6. The three series nodes of the expanded node are shown in Fig. 7 with x_1, x_2, x_3, x_4, y_1, y_2, y_3, y_4, z_1, z_2, z_3, and z_4 defined as the voltages associated with these nodes. The initial step of deriving the dispersion relation is to write the voltages V_x, V_y, and V_z at the shunt nodes, in terms of the voltages of surrounding series nodes to which they are connected. Using (13) and referring to Fig. 7, the following relations are obtained:

$$V_x = C_o\left(-z_3 T_y - y_3 T_z^{-1} - z_1 - y_1\right) \tag{31a}$$

$$V_y = C_o\left(x_3 T_z^{-1} - z_2 T_x^{-1} + x_1 - z_4\right) \tag{31b}$$

$$V_z = C_o\left(y_2 T_x^{-1} + x_4 + y_4 + x_2 T_y\right) \tag{31c}$$

where

$$C_o = \frac{1}{4\cos\left(\frac{k_o d}{2}\right)}$$

$$T_x = e^{-jk_x d}$$

$$T_y = e^{-jk_y d}$$

$$T_z = e^{-jk_z d}.$$

Next, consider a single series node connected to four surrounding shunt nodes with $\boldsymbol{V}$ as the vector of the port voltages at the series node center, and $\boldsymbol{V}'$ as the vector of node voltages at the ends of the interconnecting lines (at the center of the shunt nodes). Define $\boldsymbol{V}^i$ as the vector of voltages incident at the series node centre. Consequently,

$$\boldsymbol{V}' = \left(\boldsymbol{T}^{-1} + \boldsymbol{TS}\right)\boldsymbol{V}^i \tag{32}$$

where $\boldsymbol{S}$ is the scattering matrix of the series node and $\boldsymbol{T}$ is given as before with T_o redefined as

$$T_o = e^{-\frac{jk_o d}{2}}. \tag{33}$$

Equation (32) yields

$$\boldsymbol{V} = (\boldsymbol{I} + \boldsymbol{S})\boldsymbol{V}^i = (\boldsymbol{I} + \boldsymbol{S})\left(\boldsymbol{T}^{-1} + \boldsymbol{T}\boldsymbol{S}\right)^{-1}\boldsymbol{V}' = \boldsymbol{Q}\boldsymbol{V}' \tag{34}$$

where $\boldsymbol{Q}$ is given by

$$\boldsymbol{Q} = C_o \begin{pmatrix} 3 & 1 & 1 & -1 \\ 1 & 3 & -1 & 1 \\ 1 & -1 & 3 & 1 \\ -1 & 1 & 1 & 3 \end{pmatrix}. \tag{35}$$

The relations generated by the three series nodes are then

$$\begin{pmatrix} x_1 \\ x_2 \\ x_3 \\ x_4 \end{pmatrix} = \boldsymbol{Q} \begin{pmatrix} v_y \\ v_z T_y^{-1} \\ v_y T_z \\ v_z \end{pmatrix} \tag{36a}$$

$$\begin{pmatrix} y_1 \\ y_2 \\ y_3 \\ y_4 \end{pmatrix} = \boldsymbol{Q} \begin{pmatrix} -v_x \\ v_z T_x \\ -v_x T_z \\ v_z \end{pmatrix} \tag{36b}$$

$$\begin{pmatrix} z_1 \\ z_2 \\ z_3 \\ z_4 \end{pmatrix} = \boldsymbol{Q} \begin{pmatrix} -v_x \\ -v_y T_x \\ -v_x T_y^{-1} \\ -v_y \end{pmatrix}. \tag{36c}$$

By combining (31) and (36), an eigenmatrix equation is obtained as

$$\boldsymbol{A} \begin{pmatrix} V_x \\ V_y \\ V_z \end{pmatrix} = 0. \tag{37}$$

The eigenmatrix $\boldsymbol{A}$ is a 3 × 3 matrix with entities a_{ij} given by

$$\begin{aligned}
a_{11} &= C_o^2(12 + 2C_y + 2C_z) - 1 \\
a_{12} &= 4C_o^2 T_x^{1/2} T_y^{1/2} S_x S_y \\
a_{13} &= 4C_o^2 T_x^{1/2} T_z^{-1/2} S_x S_z \\
a_{21} &= 4C_o^2 T_x^{-1/2} T_y^{-1/2} S_x S_y \\
a_{22} &= C_o^2(12 + 2C_x + 2C_z) - 1 \\
a_{23} &= 4C_o^2 T_y^{1/2} T_z^{-1/2} S_y S_z \\
a_{31} &= 4C_o^2 T_x^{-1/2} T_z^{1/2} S_x S_z \\
a_{32} &= 4C_o^2 T_y^{1/2} T_z^{1/2} S_y S_z \\
a_{33} &= C_o^2(12 + 2C_x + 2C_y) - 1
\end{aligned} \tag{38}$$

where

$$\begin{aligned}
C_x &= \cos(k_x d) \qquad C_y = \cos(k_y d) \qquad C_z = \cos(k_z d) \\
S_x &= \sin(k_x d/2) \qquad S_y = \sin(k_y d/2) \qquad S_z = \sin(k_z d/2).
\end{aligned}$$

Consider the case where only one electric field component, namely, the E_x field (or V_x), is nonzero. Consequently, the eigen value equation reduces to $a_{11} = 0$ such that the dispersion relation becomes

$$4\cos(k_o d) = 2 + \cos(k_y d) + \cos(k_z d). \tag{39}$$

For the special case where $k_y d = 0$, (39) reduces to the dispersion relation given in [9] for propagation along the axis.

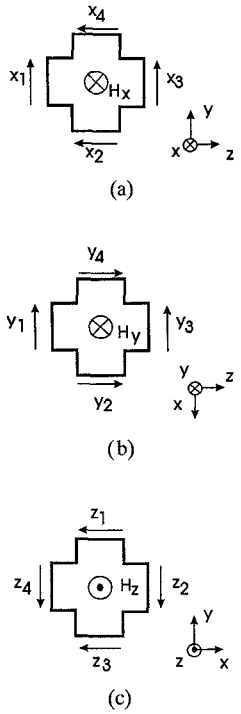

Fig. 7. Definition of variables used in derivation of dispersion relation of the 3-D expanded node. (a) H_x series node, (b) H_y series node, and (c) H_z series node.

The dispersion relation was derived again based on the currents I_x, I_y, and I_z at the series nodes. A similar procedure was followed resulting in the eigenmatrix equation

$$\boldsymbol{A}^T \begin{pmatrix} I_x \\ I_y \\ I_z \end{pmatrix} = 0 \tag{40}$$

where $\boldsymbol{A}$ is given in (38).

The eigenmatrix equations based on the shunt and series node approaches in (37) and (40) do not reveal any low-frequency spurious mode types. However, as with the shunt and series nodes, this is not a sufficient condition for the absence of spurious modes. However, the voltage and current based dispersion relations can be used to demonstrate that there are no spurious modes by the following argument.

First, as the voltage dispersion relation of (37) describes no spurious modes, any spurious modes that exist must be characterized by V_x, V_y, and V_z all equal to zero, such that (37) does not apply. Second, as the current dispersion relation of (40) describes no spurious modes, I_x, I_y, and I_z must all be zero for (40) not to apply. Combining these statements, additional spurious modes are characterized by V_x, V_y, V_z, I_x, I_y, I_z, which are all equal to zero. Given this condition, the port reflection coefficient into the shunt nodes must be -1 and the reflection coefficients into the series ports must be 1. Hence, all the interconnecting transmission lines are effectively isolated with a short circuit at one end and an open circuit at the other. As the link lines are $d/2$ long, self-consistent solutions are possible only if $k_o d$ is of the set

$$k_o d = n\pi/2 \qquad n = 1, 3, 5, \cdots.$$

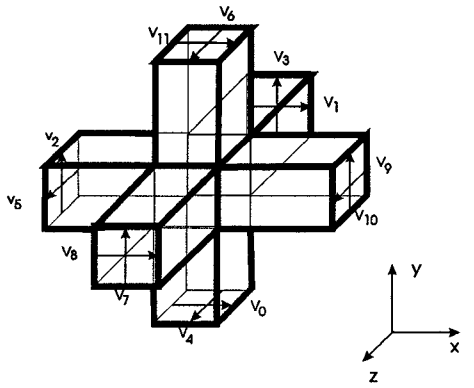

Fig. 8. 3-D TLM condensed node structure.

Since $n = 0$ is not part of the set, there are no low-frequency spurious modes. However, high-frequency spurious modes exist for $n = 1$ and $n = 3$.

VI. Symmetrical Condensed 3D-TLM Node

One disadvantage of the expanded node is that the six field components are not collocated, nor are they updated at the same time. This makes it difficult to impose arbitrary mixed boundaries. This motivated Johns to develop a different 3-D TLM node structure denoted is the "symmetrical condensed node," which consists of one central scattering center in each cube of medium rather than a set of series and shunt nodes as in the expanded node [16]. The node lattice is a cubic structure with a node spacing of d. The condensed node, sketched in Fig. 8, consists of twelve ports that connect to adjacent nodes. There is no practical lumped element equivalent circuit of the node itself.

The incident and reflected voltage in port p of the condensed node is denoted as V_p^i and V_p^r, respectively, as before. $\boldsymbol{V}^i$ and $\boldsymbol{V}^r$, the vector representations of the incident and reflected voltages, are related through the node scattering matrix $\boldsymbol{S}$ given by [16]. [See (41) at bottom of page]

The derivation of the dispersion relation for the condensed node follows a procedure similar to that used for the shunt and series nodes. An expression is written relating the port voltages of a particular node in an infinite 3-D mesh, called node c, and the voltages of the six surrounding adjacent nodes at the ports directly connected to node c. The dispersion relation will be based on an eigenmatrix equation developed for $\boldsymbol{V}^i$, the voltage incident at the center node. A spatially harmonic solution for V^i is assumed such that

$$\boldsymbol{V}^i_{i,j,k} = \boldsymbol{A}_o e^{-jk_x di} e^{-jk_y dj} e^{-jk_z dk} \tag{42}$$

when i, j, k are node indices and $\boldsymbol{A}_o$ is a constant vector.

Given the node port numbering in Fig. 8, and assuming the solution in (42), the reflected voltage at the adjacent ports can be written as

$$\boldsymbol{V}^{r\prime} = \boldsymbol{P}\boldsymbol{V}^i \tag{43}$$

where $\boldsymbol{P}$ is a 12×12 matrix with zero entries except for

$$\begin{aligned} P_{1,12} &= P_{5,7} = T_y^{-1} \\ P_{2,9} &= P_{4,8} = T_z^{-1} \\ P_{3,11} &= P_{6,10} = T_x^{-1} \\ P_{7,5} &= P_{12,1} = T_y \\ P_{8,4} &= P_{9,2} = T_z \\ P_{10,6} &= P_{11,3} = T_x \end{aligned}$$

where $T_x = \exp(-jk_x d)$, $T_y = \exp(-jk_y d)$, and $T_z = \exp(-jk_z d)$. As in the case of the shunt node, the eigenmatrix equation is given by

$$(\boldsymbol{P}\boldsymbol{S} - \boldsymbol{T})\boldsymbol{V}^i = 0 \tag{44}$$

which is of the same form as (21). Equation (44) can be simplified for special cases such as propagation along a diagonal or axis [12]; however, for the general case, no simplification has been derived.

As for the shunt node, the eigenvalues of $\boldsymbol{P}\boldsymbol{S}$ are explored. For a given $k_x d$, $k_y d$, $k_z d$ there are six unique eigenvalues for T_o that are located on the unit circle as shown in Fig. 9. There are solutions at $k_o d = 0$ and $k_o d = \pi$ which correspond to spurious solutions of type 1 and type 2 as seen in the case of the 2-D shunt and series nodes. Given that $k_o d$ is a solution, then, as indicated in Fig. 9, $-k_o d$, $\pi - k_o d$, and $\pi + k_o d$ are

$$S = \frac{1}{2}\begin{pmatrix} 0 & 1 & 1 & 0 & 0 & 0 & 0 & 0 & 1 & 0 & -1 & 0 \\ 1 & 0 & 0 & 0 & 0 & 1 & 0 & 0 & 0 & -1 & 0 & 1 \\ 1 & 0 & 0 & 1 & 0 & 0 & 0 & 1 & 0 & 0 & 0 & -1 \\ 0 & 0 & 1 & 0 & 1 & 0 & -1 & 0 & 0 & 0 & 1 & 0 \\ 0 & 0 & 0 & 1 & 0 & 1 & 0 & -1 & 0 & 1 & 0 & 0 \\ 0 & 1 & 0 & 0 & 1 & 0 & 1 & 0 & -1 & 0 & 0 & 0 \\ 0 & 0 & 0 & -1 & 0 & 1 & 0 & 1 & 0 & 1 & 0 & 0 \\ 0 & 0 & 1 & 0 & -1 & 0 & 1 & 0 & 0 & 0 & 1 & 0 \\ 1 & 0 & 0 & 0 & 0 & -1 & 0 & 0 & 0 & 1 & 0 & 1 \\ 0 & -1 & 0 & 0 & 1 & 0 & 1 & 0 & 1 & 0 & 0 & 0 \\ -1 & 0 & 0 & 1 & 0 & 0 & 0 & 1 & 0 & 0 & 0 & 1 \\ 0 & 1 & -1 & 0 & 0 & 0 & 0 & 0 & 1 & 0 & 1 & 0 \end{pmatrix}. \tag{41}$$

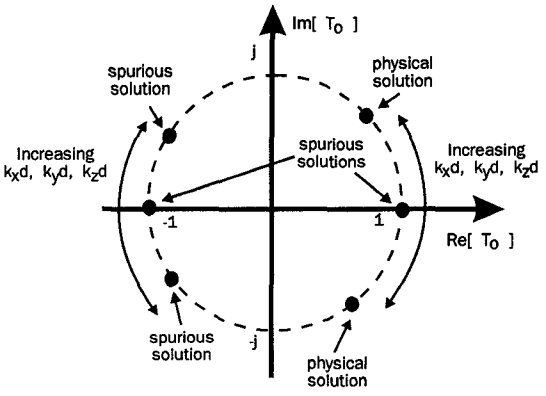

Fig. 9. Physical and spurious eigen-solutions of the 3-D condensed node in the T_o plane.

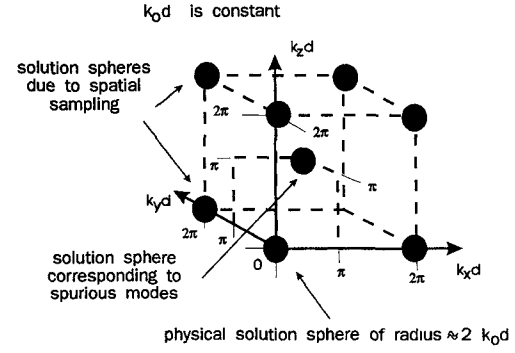

Fig. 10. Illustration of the solution spheres satisfying the dispersion equation of the 3-D condensed node.

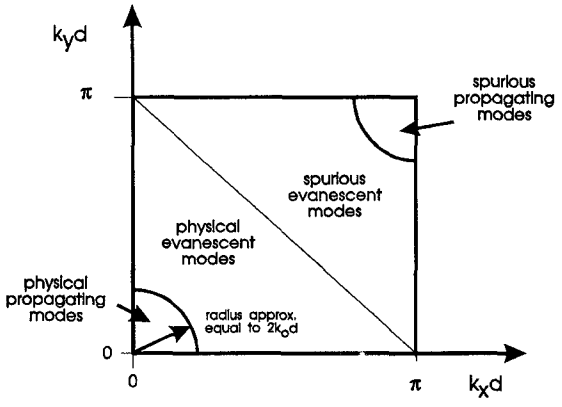

Fig. 11. Spectral regions corresponding to physical and spurious plane wave mode propagation for the 3-D condensed node.

also solutions. These four solutions correspond to physical and spurious solutions.

Insight into the properties of these solutions can be obtained by considering the problem from another perspective, where $k_o d$ is given and the possible solutions of the propagation vector that satisfy the dispersion relation are determined.

Consider the solutions for $k_x d$, $k_y d$, and $k_z d$ for a small value of $k_o d$. The solutions form a sphere with a radius of approximately $2k_o d$. Due to the spatial sampling imposed by the mesh along x, y, and z, the solution to the dispersion relation is periodic along the $k_x d$-, $k_y d$-, and $k_z d$-axis. That is, if $k_x d$, $k_y d$, $k_z d$ are solutions of the dispersion relation for a particular $k_o d$, then

$$\begin{aligned} k_x d + i \cdot 2\pi \quad & i = \pm 1, \pm 2, \cdots \\ k_y d + j \cdot 2\pi \quad & j = \pm 1, \pm 2, \cdots \\ k_z d + k \cdot 2\pi \quad & k = \pm 1, \pm 2, \cdots \end{aligned}$$

are also solution. Consequently, the solution sphere centered around $k_x d = k_y d = k_z d = 0$ is replicated in a cubic node pattern with a spacing of 2π. All these solution spheres do not contribute to spurious modes but are merely a consequence of spatial sampling. In addition to the above solutions, there is also a solution sphere centered at $k_x d = k_y d = k_z d = \pi$ as can be observed by finding the roots of the dispersion relation (44). This represents the spurious propagating mode solutions. As before, spurious solution spheres exist at intervals of 2π in $k_x d$, $k_y d$, and $k_z d$, due to spatial sampling. The total solution, assuming $k_o d$ is small, appears as a body-centered-cubic mode structure as is shown in Fig. 10.

The consequences of spurious solutions can be visualized by considering an infinite source plane in the xy plane radiating into an infinite 3-D mesh. Assume that the source plane generates a plane wave at a single frequency corresponding to k_o, and that it has a transverse dependence of $k_x x$ and $k_y y$. Using the dispersion relation, $k_z d$ can be evaluated for the radiated plane wave. The propagation characteristics of the radiated plane wave fall into one of four regions as outlined in Fig. 11. The first region for small $k_x d$ and $k_y d$ is the "physical propagating modes" region. The propagating constant, $k_z d$, for these modes is real and close to the theoretical value of

$$k_z d = \sqrt{(2 \cdot k_o d)^2 - (k_x d)^2 - (k_y d)^2}\,. \tag{45}$$

Assuming an excitation frequency such that $k_o d$ is small relative to π, the boundary of this region is approximately circular, with a radius of 2 $k_o d$. As $k_o d$ increases, the boundary will bulge slightly around the diagonal $k_x d = k_y d$.

The adjacent region is denoted as the "physical evanescent modes" region which exhibits a purely imaginary $k_z d$ that increases in magnitude with the modal index as expected in actual waveguide modes. Near the physical mode cutoff boundary, the imaginary part of $k_z d$ follows (45) accurately, provided $k_o d$ is reasonably small.

The propagation constant for modes that lie along the diagonal line given by

$$k_x d + k_y d = \pi$$

has a negative infinite imaginary component which indicates no propagation at all. When crossing this line such that

$$k_x d + k_y d > \pi\,,$$

the real part of $k_z d$ jumps to π. The modes in this region are called the "spurious evanescent modes." In this region, the magnitude of the imaginary component of $k_z d$ decreases as the mode index increases.

The boundary between the spurious evanescent and spurious propagating modes is a mirror image of the boundary separating the physical propagating and evanescent modes, and is located approximately on the curve given by

$$2k_o d = \sqrt{(\pi - k_x d)^2 + (\pi - k_y d)^2}\,. \tag{46}$$

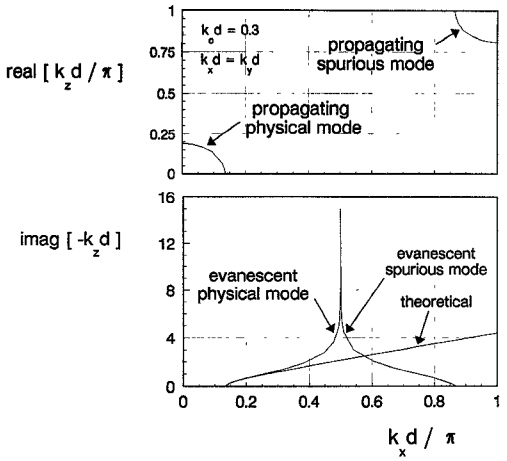

Fig. 12. Plot of $k_z d$ as a function of $k_x d$ with $k_o d = 0.3$ and $k_y d = k_x d$ [11].

The spurious propagating modes have a propagation constant of approximately

$$k_z d \approx \pi \pm \sqrt{2k_o d - (\pi - k_x d)^2 - (\pi - k_y d)^2} \qquad (47)$$

which is purely real, indicating lossless propagation. Note the constant offset factor of π. The upper sign in (47) denotes the forward propagating spurious mode, and the lower sign denotes the backward propagating mode.

Fig. 12 shows the real and imaginary parts of $k_z d$ as a function of $k_x d$ for $k_x d = 0$ to $k_x d = \pi$, with $k_y d = k_x d$. In this example, $k_o d$ is chosen to be 0.3. For small values of $k_x d$, $k_z d$ is real until the cutoff point at $k_x d = 0.42$. In the plot of the real part of $k_z d$, the theoretical solution of (45) is superimposed and is indistinguishable from the curve given by the dispersion relation (44). At $k_x d = \pi/2$, the real part of $k_z d$ jumps to a value of $= \pi$. At the cutoff point of the spurious mode, given by

$$k_x d = \pi - 0.42\,,$$

the spurious mode begins to propagate.

Consider next the curve of the imaginary part of $k_z d$ shown in Fig. 12. When $k_x d$ exceeds the cutoff point, the mode becomes evanescent. It follows the theoretical curve, given by (45), reasonable closely until $k_x d$ approaches the discontinuity at $k_x d = \pi/2$. Beyond the discontinuity, the mode becomes spurious. At the propagating spurious mode cutoff, the imaginary part of $k_z d$ becomes zero.

In summary, it is evident that modes of high spatial frequency, generated by a source that would normally attenuate very quickly with distance away from the source, may, in the TLM simulation, be represented by spurious modes that attenuate slowly or propagate without loss. This affects the simulation in several ways. First, the evanescent field distribution of the source or discontinuity is not correct. Second, the amount of coupling between physically separated ports is effected by spurious modes. Finally, the input impedance, as seen by the source, is affected since the reactance of the simulated evanescent modes is incorrect.

VII. Conclusions

In this paper, a general dispersion analysis of 2-D and 3-D TLM networks has been performed. Spurious mode solutions supported by these networks have been explored. These modes originate as a consequence of the spatial and temporal sampling process. As outlined in Section I, there are four types of spurious modes identified which were further grouped as high- and low-frequency spurious modes. As the TLM mesh is only accurate for low excitation frequencies, temporal filtering can be imposed to suppress high-frequency spurious solutions. Hence, only the low-frequency spurious modes pose a problem.

The shunt, series, and condensed nodes were found to have peculiar static spurious solutions of type 1. As stated in Section II, coupling to these modes is avoided by not including series elements or generators, and assuming initial field distributions that do not contain the spurious mode solution. Since the mode structure is linear, harmonic excitation will not couple into the static spurious solutions.

The 3-D expanded node is equivalent to Yee's FD-TD node structure, with the exception that Yee's scheme has six independent variable per node and the expanded node has twelve. Yee's FD-TD scheme does not support any spurious solutions which is a consequence of the staggered node structure. Fortunately, the spurious modes supported by the expanded node are of type 4 which are easily suppressed by temporal filtering. Freedom of low-frequency spurious modes is a strong advantage of the expanded node.

The advantages of the condensed node are that all the field components are updated at the same time and that the same location, which facilitates simulation of mixed boundary conditions and embedded devices [9]. Also, the numerical dispersion of the condensed node is significantly less than that of the expanded node [10]. However, the 3-D condensed node supports low-frequency spurious solutions of types 1 and 3 which can cause distortions in simulations. The origin of the modes can be traced to an ambiguity of high- and low-order spatial frequencies which arises due to the symmetry of the node [12]. Low-frequency spurious modes cannot easily be suppressed. An investigation into suppressing these modes is presently being undertaken.

Acknowledgment

Acknowledgment is due to K. Doucet of Lockheed Canada, as well as to the reviewers for providing helpful comments and suggestions.

References

[1] D. R. Lynch and K. D. Paulsen, "Origin of vector parasites in numerical Maxwell solutions," *IEEE Trans. Microwave Theory Tech.*, vol. 39, pp. 383–394, Mar. 1991.

[2] L. N. Trefethen, "Group velocity in finite difference schemes," *SIAM Rev.*, vol. 24, no. 2, pp. 113–135, Apr. 1982.

[3] W. E. Boyse, D. Lynch, K. Paulsen, and G. Minerbo, "Nodal based finite element modeling of Maxwell's equations," *IEEE Trans. Antennas Propagat.*, vol. 40 pp. 642–651, June 1992.

[4] P. B. Johns and R. L. Beule, "Numerical solution of 2-dimensional scattering problems using a transmission line matrix," *Proc. IEE*, vol. 118, no. 9, pp. 1203–1208, Sept. 1971.

[5] P. B. Johns, "On the relationship between TLM and finite difference methods for Maxwell's equations," *IEEE Trans. Microwave Theory Tech.*, vol. MTT-35, pp. 60–61, Jan. 1987.
[6] R. Voelker and R. Lomax, "A finite-difference transmission line matrix method incorporating a nonlinear device model," *IEEE Trans. Microwave Theory Tech.*, vol. MTT-38, pp. 302–312, Mar. 1990.
[7] Z. Chen, W. J. R. Hoefer, and M. M. Ney, "A new finite difference time domain formulation equivalent to the TLM symmetrical condensed node," in *MTT-S Dig.*, 1991.
[8] C. R. Brewitt-Taylor and P. B. Johns, "On the construction and numerical solution of transmission-line and lumped network models of Maxwell's equations," *Int. J. Numer. Meth. Eng.*, vol. 19, pp. 13–30, 1980.
[9] W. J. R. Hoefer, "The Transmission Line Matrix (TLM) method," in *Numerical Techniques for Microwave and Millimeter-Wave Passive Structures*, T. Itoh, Ed. New York: Wiley 1989, ch. 8.
[10] J. Nielsen and W. J. R. Hoefer, "A complete dispersion analysis of the condensed node TLM mesh," *IEEE Trans. Magn.*, vol. 27, pp. 3982–3985, Sept. 1991.
[11] J. S. Nielsen, "Spurious modes of the TLM-condensed node formulation," *IEEE Microwave Guided Lett.*, vol. 1, pp. 201–203, Aug. 1991.
[12] ——, "TLM analysis of microwave and millimeter wave structures with embedded nonlinear devices," Ph.D. dissertation, Univ. Ottawa, 1992.
[13] N. R. Simons and E. Bridges, "Equivalence of propagating characteristics for the transmission-line matrix and finite-difference time domain methods in two dimensions," *IEEE Trans. Microwave Theory Tech.*, vol. 39, pp. 354–357, Feb. 1991.
[14] S. Akhtarzad and P. B. Johns, "Solution of 6-component electromagnetic fields in three space dimensions and time by the T.L.M. method," *Electron. Lett.*, vol. 10, pp. 535–537, Dec. 12, 1974.
[15] K. S. Yee, "Numerical solution of initial boundary value problems involving Maxwell's equations in isotropic media," *IEEE Trans. Antennas Propagat.*, vol. AP-14, pp. 302–307, May 1966.
[16] P. B. Johns, "A symmetrical condensed node for the TLM method," *IEEE Trans. Microwave Theory Tech.*, vol. MTT-35, pp. 370–377, Apr. 1987.

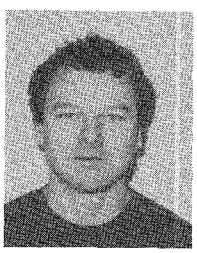

John S. Nielsen (M'86) received the B.A.Sc. and M.A.Sc. degrees in 1981 and 1984, respectively, from the University of Toronto, and the Ph.D. degree from the University of Ottawa; his thesis research involved developing the TLM method for nonlinear electromagnetic circuit problems.

From 1983 to 1986 he was a Researcher Engineer at the Defence Research Establishment Ottawa. Since 1986 he has worked at Lockheed Canada Inc. with the electronic countermeasures group analyzing and designing specialized optical and microwave components.

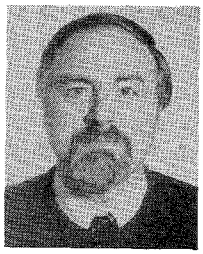

Wolfgang J. R. Hoefer (F'91) received the Dipl.-Ing. degree in electrical engineering from the Technische Hochschule Aachen, Germany, in 1965, and the D. Ing. degree from the University of Grenoble, France, in 1968.

During the academic year 1968–1969 he was a Lecturer at the Institut Universitaire de Technologie de Genoble and a Research Fellow at the Institut National Polytechnique de Grenoble, France. In 1969 he joined the Department of Electrical Engineering, the University of Ottawa, Canada where he was a Professor until March 1992. Since April 1992 he has held the NSERC/MPR Teltech Industrial Research Chain in RF Engineering in the Department of Electrical and Computer Engineering, The University of Victoria, Canada. During sabbatical leaves, he spent six months with the Space Division of AEG-Telefunken in Backnang, Germany (now ATN), and six months with the Electromagnetics Laboratory of the Institut National Polytechnique de Grenoble, France, in 1976–1977. During 1984–1985 he was a Visiting Scientist at the Space Electronics Direcotorate of the Communications Research Centre in Ottawa, Canada. He spent a third sabbatical year in 1990–1991 as a Visiting Professor at the University of Rome "Tor Vergata" in Italy, the University of Nice–Sophia Antipolis in France, and the Technical University of Munich in Germany. His research interests include numerical techniques for modeling electromagnetic fields and waves, computer-aided design of microwave and millimeter-wave circuits, microwave measurement techniques, and engineering education. He is the co-founder and managing editor of the *International Journal of Numerical Modelling.*

Dr. Hoefer is a Fellow of the Advanced Systems Institute of British Columbia.